THE JOURNAL OF PHYSICAL CHEMISTRY LETTERS
A JOURNAL OF THE AMERICAN CHEMICAL SOCIETY

pubs.acs.org/JPCL Letter

Structural and Electronic Properties of p(2×2) Phosphorus Layer on Au(100)

Yann Girard,* Mehdi Bouatou, Abhishek Karn, Cyril Chacon, Ian-Evan Michel, Yannick J. Dappe, Alexander Smogunov, Yves Garreau, Alina Vlad, Alessandro Coati, and Jérôme Lagoute

Cite This: J. Phys. Chem. Lett. 2026, 17, 9797−9806 Read Online

ACCESS | Metrics & More | Article Recommendations | Supporting Information

ABSTRACT: We present the superstructure formed during phosphorus deposition on the reconstructed Au(100)-hexagonal surface together with its electronic properties. Scanning tunneling microscopy and spectroscopy combined with X-ray diffraction are compared to first-principles calculations. All these results consistently indicate a p(2×2) phosphorus structure with P atoms in hollow sites above a strained Au(100) surface. At intermediate coverage, Au(100)-hexagonal domains coexist with the p(2×2) superstructure. For full coverage, the reconstruction is completely lifted. Structure factors deduced from theoretical calculations and those measured by diffraction are in excellent agreement and demonstrate that P atoms induce significant Au strain which promotes a 0.2 Å outward relaxation associated with the quadrimerization of the underlying Au atoms. From the point of view of an electronic density perspective, a peak at 3.6 eV is observed in the unoccupied states, which is also supported by density functional theory. This is explained by a transfer of electrons from the Au surface to the P atoms.

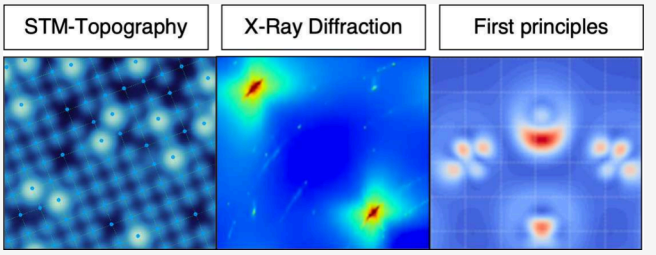

Black phosphorus (black-P) thin films bridge the gap between graphene and transition-metal dichalcogenides due to their high carrier mobility and tunable band gap (0.3 eV in bulk to 2 eV in monolayer). A few layers of black-P exhibit an adjustable electronic band gap that depends on the number of layers, making them of high interest in optical or electronic engineering.[1,2]

It has been theoretically predicted that phosphorene - a single layer of phosphorus atoms - exhibits a large number of possible 2D-allotropes (2D-PA).[3] Each of these allotropes features modulable electronic properties that vary according to their atomic structure as well as the size or shape of low-dimensional phosphorene nanostructures.[4] To date, only three allotropes have been experimentally synthesized: black, blue, and violet phosphorus (for a review, see L. Ding et al.[5]) The two main processes used are exfoliation for black-P and violet-P and molecular beam epitaxy (MBE) or chemical vapor deposition (CVD) methods for blue-P. The current challenge in the field is to achieve novel physical properties in 2D-PA[6,7] and to develop methods for large-scale production. This can be accomplished by exploring new 2D-PA, which currently involves growing phosphorus on various substrates to discover new phases and thus new physical properties.

It has been proposed that to obtain the various allotropes, it is necessary to use one of the fundamental properties of the bonds between P atoms: its anisotropy; namely, it is rigid in the plane and flexible in the perpendicular direction. We can play with this property by adjusting the stress, which can be controlled by the substrate crystallographic orientation or chemical composition. The resulting allotropes are expected to exhibit various structures and electronic properties, in the same way as the effects of substrate-induced stress on molecular assemblies,[8,9] silicene on Ag or Al,[10] or step density on graphene.[11]

For instance, black-P (blue-P) exhibits a rectangular (hexagonal) lattice structure, making it particularly compelling to employ substrates with similar symmetry, such as the (110) or (111) surfaces of face-centered cubic (FCC) metals (e.g., Ag, Au, Cu, etc.). In this context, experimental efforts have encountered significant challenges, including substrate alloying and the limited lateral extension of the phosphorus films which often form narrow nanoribbons rather than continuous layers.[12−14] Concerning hexagonal surfaces, excepted P/Cu(111),[15] the other systems exhibit phosphorene subunits connected by substrate atoms,[16] or various unexpected P structures such as stripes or pentamers.[17,18]

To understand the formation of these phosphides and thereby determine the physical barrier that prevents 2D-PA formation beyond a few nanometers, it is essential to investigate the initial growth stages on different substrates.

Received: June 20, 2026
Revised: August 6, 2026
Accepted: August 7, 2026
Published: August 14, 2026

https://doi.org/10.1021/acs.jpclett.6c02046
J. Phys. Chem. Lett. 2026, 17, 9797−9806

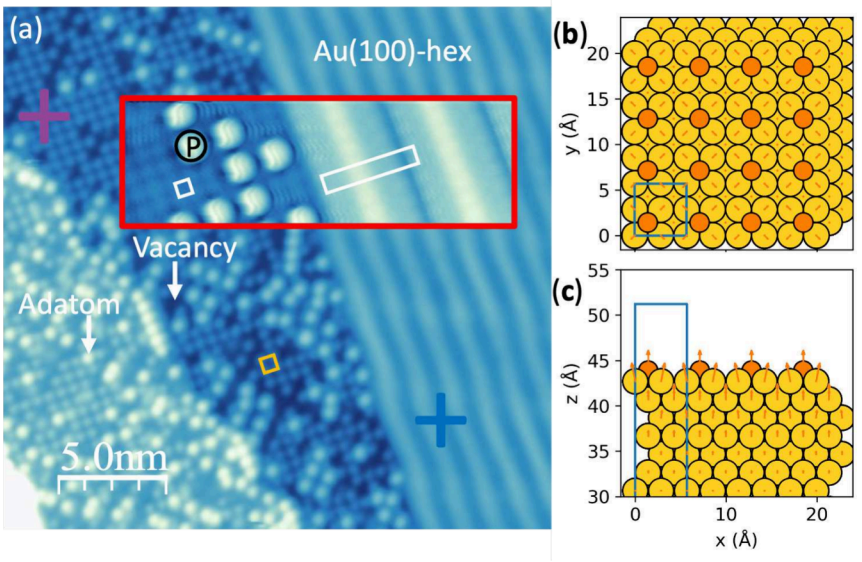

Figure 1. (a) STM image (25 nm × 25 nm) of low phosphorus coverage on Au(100) after a few minutes of deposition of P at 200 °C, followed by imaging at 4 K. Two distinct regions are observable: in the left region, two Au(100) terraces display P atoms arranged in a p(2×2) superstructure (indicated by the orange square), with visible point defects, including P vacancies (darker spots) and P adatoms (bright protrusions); in the right region the characteristic Au reconstruction lines of Au(100)-hex phase are evident. A magnified area (highlighted by the red rectangle, 6 nm × 2 nm) at a reconstruction domain boundary reveals an apparent p(5×1) superstructure of Au(100) and a quasi P-depleted zone, clearly showing P atoms occupying hollow sites relative to the unreconstructed (100) plane (a p(1×1) unit cell is indicated by the white square). (b) and (c) Top and side views of the structurally optimized p(2×2) model. Gold and orange spheres represent Au and P atoms, respectively. The arrows indicate the displacements of the atoms from their initial positions, scaled by a factor of 12 for clarity. The blue box represents the unit cell used for the calculations.

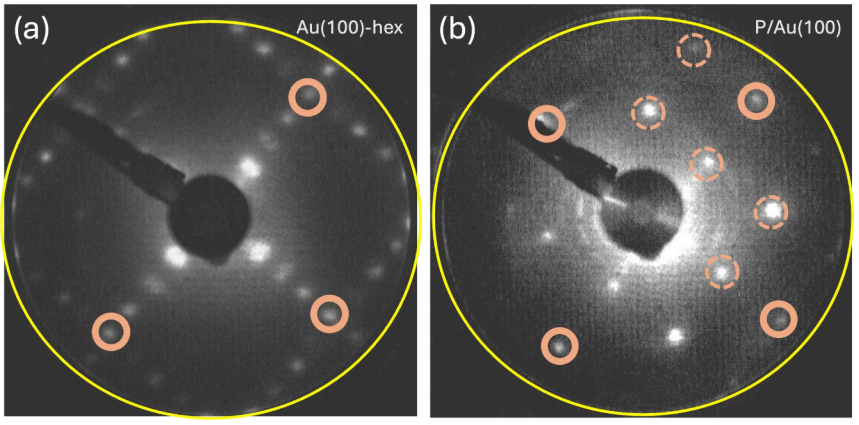

Figure 2. LEED patterns of Au(100)-hex and P/Au(100). (a) Clean Au(100)-hex. (b) p(2×2) diffraction after a few minutes of P evaporation at 240 °C followed by 1 h annealing at 260 °C. Full circles labeled Au(100) spots. Dotted circles labeled the superstructure. The beam energy is 45 eV.

Here, we present measurements and calculations performed on the phosphorus-Au(100) system, following previous experimental studies conducted on Au(111),[19,20] on Cu_30_2,[21] or extending those on Au(100)[22] where a p(2×2) square symmetry structure has been shown to be a precursor of a denser hexagonal layer. Thus, we have precisely determined the atomic structure of this p(2×2)-P superstructure and its resulting electronic properties (EPs). These results have been obtained through a combination of scanning tunneling microscopy (STM), scanning tunneling spectroscopy (STS), and grazing incidence X-ray diffraction (GIXD), combined with first-principles density functional theory (DFT) calculations.

To study the early stages of growth, we limited the phosphorus coverage to approximately a few ten percents (proportion of the covered surface area). Thus, after evaporation for a few minutes at 200 °C, a STM image acquired at 4 K allows direct comparison between P-rich areas and those without phosphorus. A large-scale STM image (reported in the SI) shows the clear separation between uncovered Au(100)-hex terraces and areas covered with phosphorus structures. These areas cover approximately 50% of the surface.

Figure 1a shows an image with quasi-atomic resolution. The boundary between a phosphorus-free domain on the right and a domain exhibiting a periodic superstructure with a square symmetry on the left is clearly visible.

The structure which exhibits quasi-parallel lines on the P-free domain corresponds to the Au(100) surface reconstruction, which we will refer to as Au(100)-hex hereafter.[23] The

https://doi.org/10.1021/acs.jpclett.6c02046
J. Phys. Chem. Lett. 2026, 17, 9797−9806

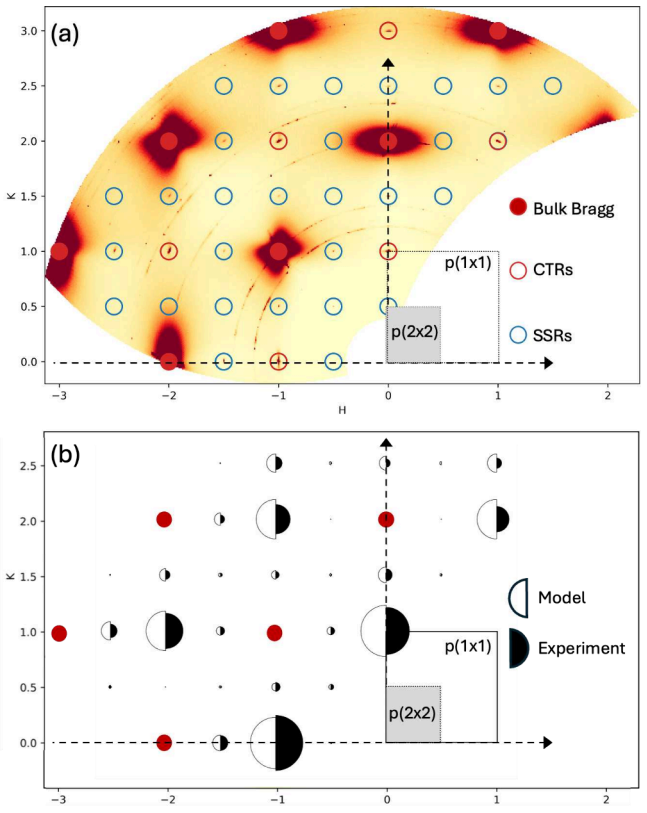

Figure 3. (a) (H, K, L = 0) map of P/Au(100) integrated between L = ±0.05. The color scale represents the number of photons per pixel per integration time. Bulk Bragg peaks (disks) and Crystal Truncation Rods (CTRs) (circles) are highlighted in red. p(2×2) surface superstructure rods (SSRs) are shown in blue. Bragg spots are highly intense, for example (−2, 0, 0) or (−1, 1, 0); CTRs are also intense, such as (−1, 0, 0) or (−1, 2, 0); faint spots, corresponding to the p(2×2)-P superstructure, are visible, for example, (−1.5, 0, 0) or (−2.5, 1, 0). Note the quasi-extinctions at half-integer positions, for example, (−1.5, 0.5, 0). The gray square indicates the p(2×2) reciprocal unit cell. (b) Top view of $L \simeq 0$ reciprocal space. SFs of in-plane reflections are represented as half-circles, with radii proportional to their modulus. The right halves correspond to experimental data, while the left halves are derived from simulations using the relaxed p(2×2) model.

lines are parallel to the ⟨110⟩ directions and exhibit a periodicity close to a p(1×5) superstructure (six-atomic rows of the top layer fit onto five-atomic rows of the underlying substrate), as shown by an atomic resolution image in the red inset. A white rectangle indicates this apparent unit cell.

Note that the lines present a slight undulation and, in fact, the actual unit cell has a larger period and would be close to p(5×20) or even c(28×48). The atomic structure of this complex reconstruction is still under investigation and, in summary, it is accepted that it results from a quasi-hexagonal contraction of the surface plane due to the fact that, phenomenologically speaking,[24] all atoms should be surrounded as much as possible by other atoms. This surface plane is 25% denser than a bulk (100) plane[25] and its quasi-hexagonal symmetry closely resembles a (111) plane.

We can recall that, on an Au(111) crystal, P atoms deposition performed at room temperature with low coverage exhibits (after annealing for 1 h at 150 °C) some patches of $(\sqrt{3} \times \sqrt{3})$R30° superstructure all over the surface.[20] Here, on Au(100)-hex, this growth mode is not observed. This suggests that P atoms diffuse easily across the surface until they encounter a step edge or a grain boundary connecting two reconstructed domains.

Indeed, an identical growth mode has been observed, for example, during tellurium adsorption on Au(100)-hex via step-edge retreat.[26] Once trapped by those defects, P atoms induce a strong restructuring of the surface; that is, the Au(100)-hex is locally destroyed and a Au(100) plane is stabilized by P adsorption.

A possible scenario is as follows. The adsorbed P atom density (which is greater near step edges or grain boundaries) must be sufficient to modify the local electronic environment and, consequently, the local stress. Thus, although the atomic mechanisms are unknown, patches of P atoms may favorably replace the atomic overdensity of the gold surface plane near these defects. One may wonder where the excess Au atoms that formed the quasi-hexagonal reconstruction have gone. Since the deconstruction occurs from extended defects, the constitutive atoms become free to diffuse, and it is accepted that they cluster together along steps, as shown in the case of Cu or S on Au(100)-hex.[27,28] Other examples of the Au(100)-hex instability against adsorption are largely encountered; we can cite, for example, some very reactive elements such as chlorine or bromine,[29] but also Te,[26] S,[30] Fe,[27] or various thiols.[31] Note that, due to the large number of atoms that constitute the Au(100)-hex surface (we must take into account, not only the 25% extra atoms of the surface plane, but also several atomic planes below the surface),[24,25] no theoretical DFT prediction regarding its stability against adsorption exists to date. Nevertheless, concerning specifically low-index Au surfaces, we can note that the phosphorus adsorption, even at very low coverage, is always accompanied by the removal of gold atoms, such as the disappearance of the Au(111) herringbone reconstruction[32] or removal of Au(110) rows.[33]

The left side of Figure 1a is covered with a square symmetry superstructure (indicated in orange on the central terrace) with a size of 5.76 Å × 5.76 Å equal to twice the Au−Au interatomic distance of 2.88 Å (see also Supporting Information (SI)). It is noticeable that, on one hand, this structure presents some vacancies and even some vacancy islands (see a zoom in inset), and on the other hand, it is decorated with adatoms that appear to be randomly distributed but which may also serve as precursors to the formation of a $(\sqrt{2} \times \sqrt{2})$R45° second layer of phosphorus, as demonstrated by certain locally ordered arrangements in lines or squares (see also SI). In order to determine the position of P atoms on the Au(100) surface, the red inset shows a zoom into a vacancy island at the left edge of an Au(100)-hex domain. This reveals the p(1×1) surface of a gold plane (indicated by a white square) as well as atoms in hollow positions. These atoms, which we assume to be phosphorus atoms, form the p(2×2)-P structure that almost entirely covers the terraces.

To confirm the local p(2×2)-P structure observed by STM and its relationships with the deconstructed substrate, i.e. the in and out of plane Au and P atom positions relative to the Au substrate, we propose a model based on DFT calculations. This model has been fully optimized by DFT using the QUANTUM ESPRESSO package.[34,35] Details about the computational methods are given in SI. Note that an alternative model has also been explored (see SI). While preserving the experimentally observed square symmetry, we tested a c(2×2) structure (equivalent to a $(\sqrt{2}\times\sqrt{2})$-R45°

https://doi.org/10.1021/acs.jpclett.6c02046
J. Phys. Chem. Lett. 2026, 17, 9797−9806

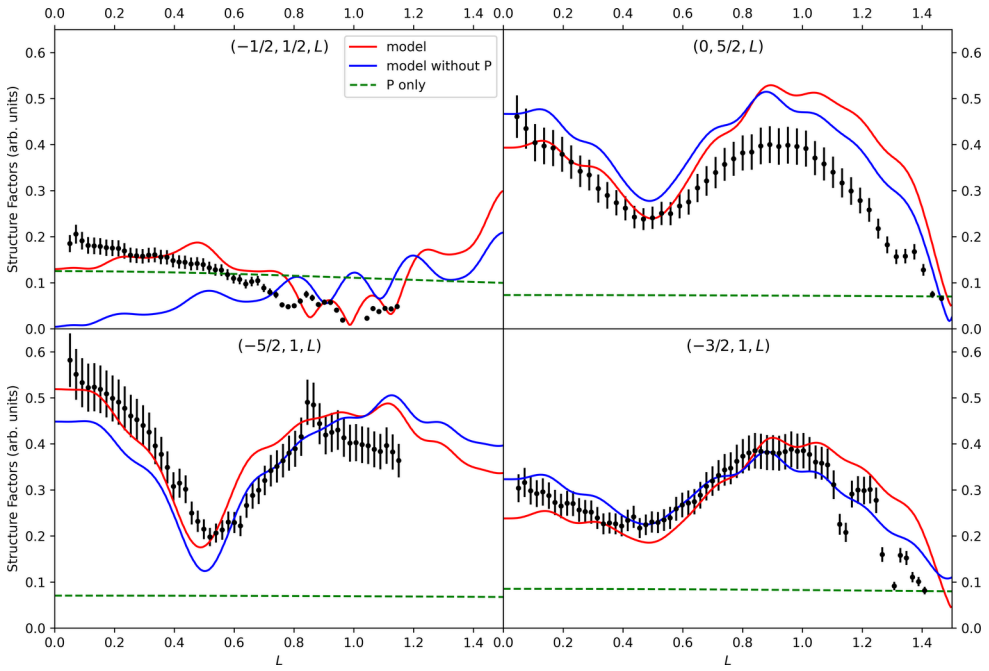

Figure 4. Comparison of SFs between experimental L scans along various p(2×2) rods of P/Au(100) and calculated scans. The calculated SFs, based on the theoretical p(2×2) model, are represented by continuous red lines. The blue line corresponds to the model excluding the contribution of P atoms, while the green line represents the model excluding the contribution of Au atoms.

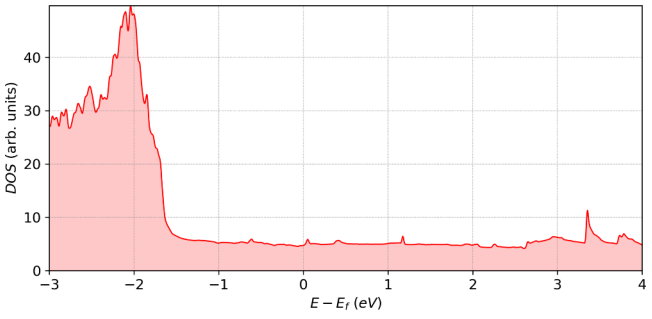

(a) Au(100) slab without phosphorus atoms.

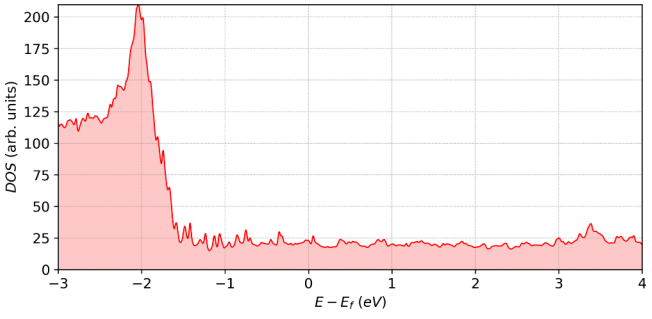

(b) p(2x2) model.

Figure 5. Comparison between the total DOS of a theoretical Au(100) slab (a) and the proposed p(2×2) model (b).

structure). After relaxation, we found that this structure is stable and exhibits vertical relaxation of Au atoms. However, and this is a critical point, it shows no in-plane relaxation. Consequently, the diffraction rods calculated based on this alternative model clearly cannot reproduce our experimental GIXD measurements. So, this model has been rejected. Regarding the retained p(2×2) model, a slab of 18 layers of Au(100) serving as a substrate has been preemptively optimized, keeping the 6 bottom layers fixed to the bulk positions. Then, P atoms have been added at 1.2 Å above the surface and have been optimized along with the top 6 layers of Au. Those P atoms will ultimately lay 1.22 Å above the gold surface after optimization. This last optimization is shown in Figure 1b and c using arrows indicating the displacements (×12) of the atoms from their initial positions. Adding P atoms on the surface leads to an uplift of the topmost Au layers. The gold atoms surrounding the P atom move away from it by 0.056 Å in the surface plane and move up uniformly by 0.2 Å in the out-of-plane direction. Gold atoms in the plane below have no planar displacement due to symmetry but move upward from 0.015 Å to 0.13 Å depending on the site. It is known that the hexagonal reconstruction not only involves atoms of the surface plane, but also, to a lesser extent, those of the underlying planes. It follows that one should also expect that the replacement of the gold plane by a phosphorus plane does not completely relax the bulk deformations. The interaction of P atoms in hollow positions with the four underlying Au atoms is so strong that the latter move symmetrically away from the center, creating a quadrimerization of the Au(100) first surface plane. We can definitively conclude that, at a local 0.5 ML coverage (relative to an Au(100) plane), the p(2×2)-P structure is the stable relaxed configuration adopted by the system. This structure serves as a precursor to higher-coverage superstructures (e.g., toward a BlueP-Au network,[22]), though this is beyond the scope of the current paper.

Before turning to the electronic properties reported below and in order to test the accuracy of those calculated results, we have performed grazing incidence X-ray diffraction on a full p(2×2) layer. Then, we have compared experimental structure factors (SFs) with those based on the calculated atomic positions obtained after a full relaxation of the model.

https://doi.org/10.1021/acs.jpclett.6c02046
J. Phys. Chem. Lett. 2026, 17, 9797−9806

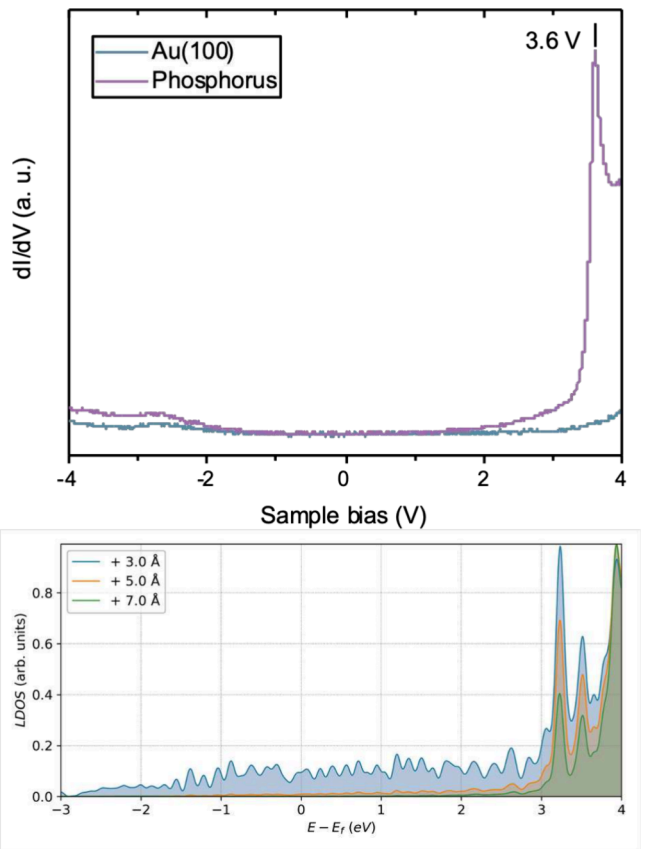

Figure 6. STS data comparing differential conductance (dI/dV) as a function of sample bias between an Au(100)-hex domain (blue marker) and a p(2×2) phosphorus structure (purple marker) indicated in Figure 1a. A characteristic spectroscopic feature at approximately 3.6 eV above the Fermi level serves as a distinctive signature of P-covered areas. LDOS are calculated at different distances above a P atom. The overall decrease of the LDOS with the distance is more pronounced for states coming from Au rather than for P.

We have increased the phosphorus deposition amount and performed LEED pictures before and after P adsorption until the full disappearance of gold reconstruction. The LEED pattern presented in Figure 2a, measured as a reference on the clean Au(100)-hex surface, is characteristic of the quasi-p(5×1) superstructure.[23,28] Once the deconstruction is total, (1/2,1/2) spots appear clearly into the pattern reported in Figure 2b, which corroborates our assumption. We can note that the coverage is still low because there is no signature of blue-P islands as observed with a greater deposition time.[22] It is important to note that point because, even if LEED gives information about the symmetries of a structure, it is difficult to extract the in-plane atomic positions (as STM often could) or the vertical position (just as STM cannot do it either) because of well-known electron multidiffraction (or convolution and electronic tip effects).

First, we present the experimental results of the X-ray diffraction. In the following, the (H, K, L) coordinates of a reciprocal space point are adapted to a FCC crystal with an unreconstructed (100) surface; that is, the in-plane symmetries and lattice constants are identical to that of a bulk (100) plane. Indexes H and K refer to a reciprocal space vector lying in the plane of the sample surface, and L refers to the out-of-plane component. In this representation, Bragg peaks are obtained for $H + K + L$ even (cf. SI).

Figure 3a shows a 2D cut of the reciprocal space in the (H, K, $L = 0$) plane (an in-plane map). Three distinct families of diffraction peaks are observed. The more intense ones are bulk Bragg peaks where, for integer values of H and K, their sum $H + K$ is even. Crystal Truncation Rods (CTRs) which cut this plane for all (H, K) couples are less intense for $H + K + 1$ even, i.e. in anti-Bragg positions (for example, ($H = -1$, $K = 0$) or ($H = 1$, $K = 2$)). The third family is obtained for half integer values (for example, (−1.5, 0), (−2.5, 1) or (0, 2.5)). These peaks correspond to Superstructure Surface Rods (SSRs) and are the fingerprints of what seems to be a p(2×2). Regarding gold (red circles), note that the map is invariant under a $\pi/2$ rotation, as expected for a 4-fold symmetry. If the motif of the p(2×2) was constituted by only one atom, we should have observed diffracted intensity in this map for all half-integer values of H and K. But, for certain expected positions, there is a nearly complete extinction, for example: (−1.5, 1.5) or (0.5, 2.5). Therefore, to explain why some spots related to a p(2×2) are nearly extinct, we must consider interference effects between the atomic positions in the superstructure and the underlying crystal. Thus, we have measured 16 CTRs and 20 SSRs and obtained experimental SFs which are reported in Figure 3b for $L = 0$ and Figure 4 for some characteristic nonequivalent SSRs.

Once experimental SFs are obtained, we can compare them with those calculated from atomistic simulations. The key result presented below is that the modulations observed along the CTRs are primarily induced by the quadrimerization of Au atoms beneath the P atoms associated with a uniform outward

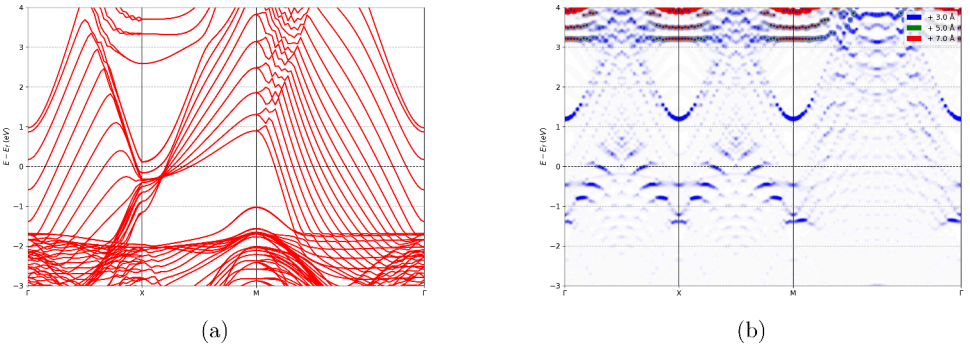

Figure 7. Comparison between (a) the band structure of the bare Au(100) slab and (b) the band structure weighted by the LDOS contribution for the p(2×2) model at different distances above a P atom.

https://doi.org/10.1021/acs.jpclett.6c02046
J. Phys. Chem. Lett. 2026, 17, 9797−9806

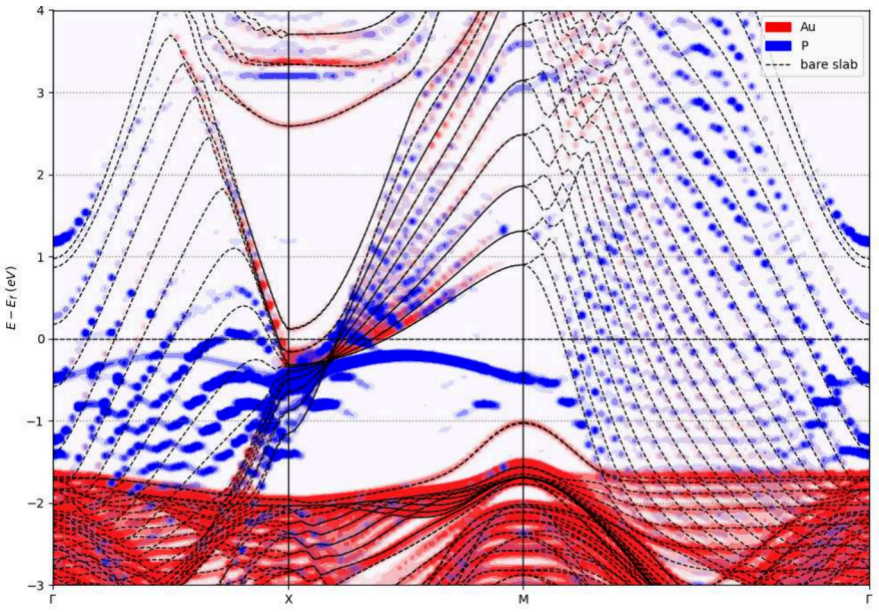

Figure 8. Band structure of the p(2×2) model unfolded into the Brillouin zone of the bare Au(100) slab. The band structure of the bare Au(100) slab is superimposed in dashed black lines for comparison. The contribution of gold and phosphorus atoms to the band structure of the p(2×2) model is highlighted in red and blue, respectively.

relaxation of the first Au(100) plane, forming a p(2×2) superstructure, as shown previously in Figure 1.

Once the coordinates of the P and Au atoms have been obtained by DFT, we used the ROD software (see Methods in the SI) to compare the calculated SFs to the experimental ones.

Some results are reported in Figure 4. One immediately observes that, without any refinement of the atomic positions calculated by the p(2×2) model, all of the modulations present in the experimental curves are reproduced in the corresponding calculated ones.

It is also clear that dips consistently occur at half-integer values of L, which is a signature of significant vertical relaxation of the topmost surface layer, i.e. 0.20 Å. Moreover, we can now compare quantitatively the experimental and the calculated L = 0 in-plane SFs. This is reported in Figure 3b. The comparison is excellent, and the calculations reveal even the faintest spots, which had appeared nearly extinct. Finally, it is important to note that the atomic scattering factor of gold is nearly five times greater than that of phosphorus, so only the displacements of the gold atoms contribute significantly to the modulations of the SFs. Here, it is clearly the case as shown in Figure 4, where the contributions of P (green dotted line) and Au (blue line) atoms to the SFs have been separated.

It is worth noting that the vertical position of phosphorus atoms has a very limited effect on the structure factors. Consequently, the comparison between our experimental results and the calculated ones is primarily constrained by the accuracy of our calculations. It is generally accepted that the precision of calculations using the PBEsol functional without any van der Waals correction (described in the SI) is approximately 0.01 to 0.05 Å. To achieve better accuracy in determining the positions of gold atoms, it would be interesting to use a point detector, which offers a 10-fold improvement in angular resolution compared to the 2D-XPAD detector we employed. Additionally, slightly relaxing the calculated Au positions could help refine the atomic coordinates. This approach would likely enhance the precision to approximately 0.001 to 0.01 Å for a point detector and could reduce the uncertainties in the determined atomic positions.

Therefore, we can resume those results by assuming phosphorus−gold interaction is the "driving force" for the Au surface relaxations, but its atomic contribution to the diffraction patterns is almost negligible.

Given that the calculated relaxed atomic configurations are well-supported by the GIXD measurements, we proceeded to compute the electronic properties, including the density of states (DOS) and local density of states (LDOS) (see Computational Methods in the SI). First, we present the DOS calculation results. Next, we compare the experimental STS spectrum to the LDOS. Finally, we further investigate the electronic properties by analyzing the projected density of states (PDOS) and integrated local density of states (ILDOS).

The DOS of the bare Au(100) slab and the p(2×2) model are shown in Figure 5. They are very similar, except for the peaks between 3 and 4 eV. The total DOS is naturally dominated by gold atoms, hence the strong similarity between the DOS of the two systems. For the bare Au(100) slab, the peak at 3.4 eV in Figure 5a is due to a flat band at the X point, which can be seen in the corresponding band structure in Figure 7a. This peak is then decomposed in the p(2×2) model into smaller peaks after hybridization with the phosphorus atoms, as shown in Figure 5b.

In order to characterize the local electronic properties of the p(2×2) structure, we measured by STS the differential conductivity, dI/dV, on each of the domains (with and without P) described in Figure 1a. These measurements are reported in Figure 6 and compared to calculated LDOS.

Concerning the experimental measurements, we observe that the occupied states ($V < 0$) exhibit almost the same characteristic shoulder in both domains. This shoulder originates mainly from the bulk Au electronic structure and is unaltered by the Au surface plane (see also below for our computational results). Since this shoulder is also present in the p(2×2) areas, it follows that the coupling between this new

https://doi.org/10.1021/acs.jpclett.6c02046
J. Phys. Chem. Lett. 2026, 17, 9797−9806

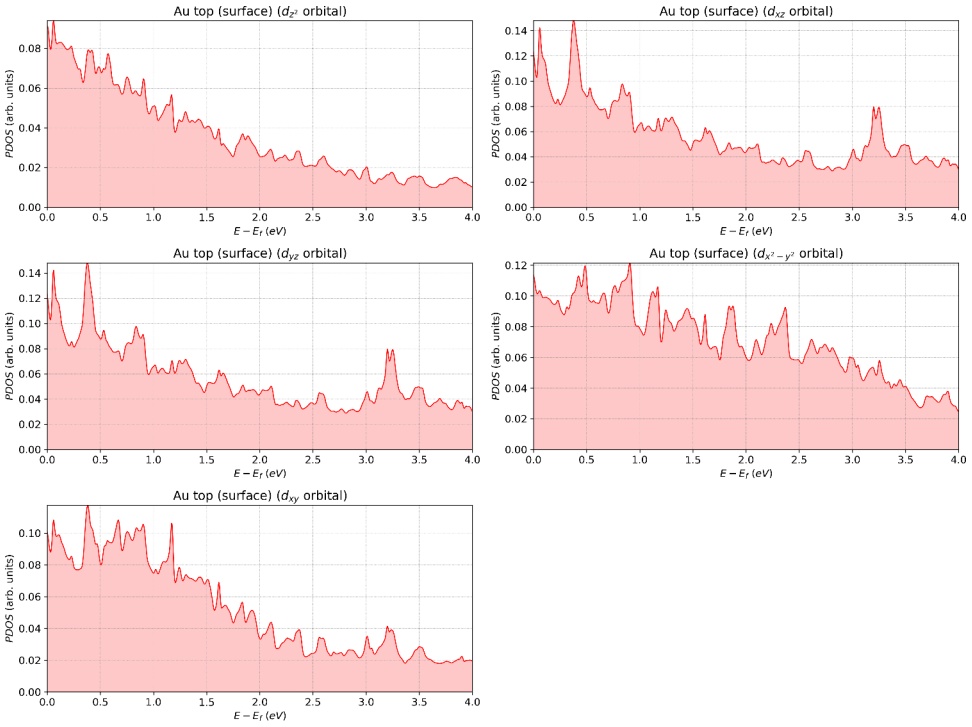

(a) PDOS on the different d orbitals of the Au top surface atoms.

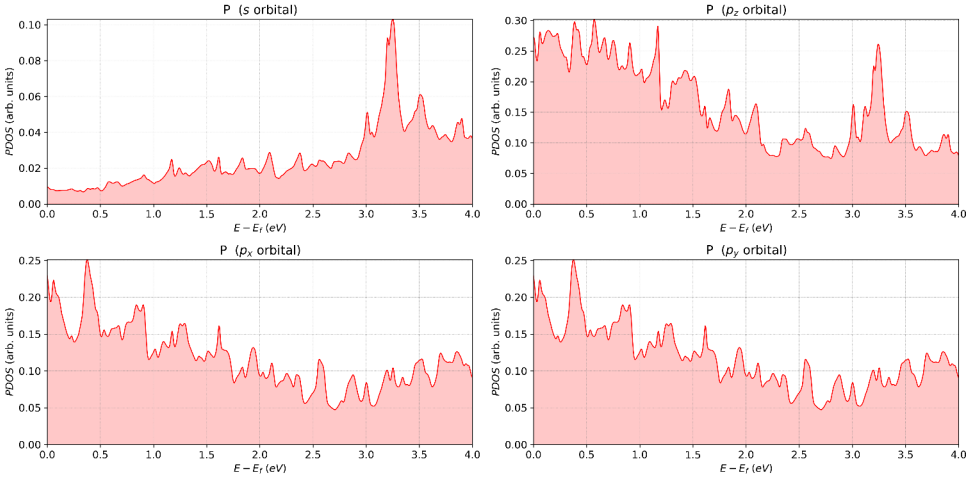

(b) PDOS on the orbitals of the P atom.

Figure 9. PDOS for the p(2×2) model.

interface and the bulk is rather small. Contrarily, for the unoccupied states ($V > 0$), it is obvious that the peak around 3.6 eV appears only in the p(2×2) region. This peak is not related to field-emission (the experimental Au(100) work-function is equal to 5.47 eV))[36] nor to image potential states that are above 5 eV.[37]

This peak originates from interactions between P atoms and the gold substrate, as demonstrated by the DFT calculations presented below.

In order to compare the STS spectrum with the theoretical DOS, the LDOS is calculated and reported in Figure 6. The LDOS is calculated in a box above the phosphorus atoms with a height varying from 3.0 to 7.0 Å. For more details about the calculation, see Computational Methods in SI. To better compare to the given STS spectrum, one should consider truncating the LDOS up to 3.3 eV. The pronounced peak observed in the STS spectrum can indeed be attributed to the first and sharp peak at approximately 3.2 eV in the LDOS of the model. This value is slightly lower than the experimental value of 3.6 eV. This aside, the sharpness and height of this peak are very similar to those of the peak in the STS spectrum. A second peak right of this first peak can be seen in the LDOS, as one can also guess a second peak in the STS spectrum above 4 eV. An even bigger peak is observed around 3.9 eV in the LDOS, but the STS spectrum does not go that high in energy to confirm or infirm the existence and shape of these higher energy peaks. It is known that DFT tends to underestimate band gaps, so we can rightfully expect the calculations to underestimate the energy of unoccupied states. With this in mind, the peak at 3.2 eV is more likely to match the main peak in the STS spectrum at 3.6 eV.

https://doi.org/10.1021/acs.jpclett.6c02046
J. Phys. Chem. Lett. 2026, 17, 9797−9806

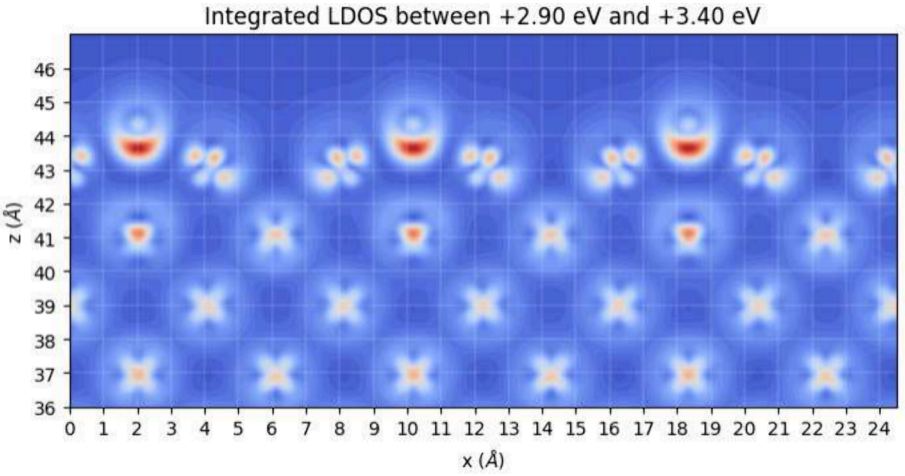

Figure 10. Vertical plane cut along the $\sqrt{2}$ direction of the integrated LDOS of the p(2×2) model around the peak at 3.2 eV. The topmost three atoms are the phosphorus atoms, and the bottom four layers of atoms are the gold atoms.

In order to gain more insights into the origin if this peak, we have performed band structure calculations. In Figure 7a we show the result for bare Au(100) along the high-symmetry path $\Gamma - X - M - \Gamma$ of the Brillouin zone. Figure 7b shows the folded[38] band structure of the p(2×2) model weighted by the LDOS contribution.

We can see that there are several flat bands between 3 and 4 eV which are responsible for the peaks in the LDOS. For the p(2×2) model (Figure 7b), the very flat band around 3.2 eV at the Γ point is responsible for the sharp peak in the LDOS at this energy (we recall that STS is essentially sensitive to electron tunneling at this point, i.e. without lateral momentum transfer).

Using the unfolding code 'unfold.x' written and maintained by Pietro Bonfa[39] and based on the method described in the article by Popescu and Zunger,[38] we have unfolded the band structure of the p(2×2) model to compare it with the band structure of the bare Au(100) slab. To better visualize the differences between the two band structures, the band structure of the p(2×2) model has been projected onto gold in red and phosphorus in blue, as shown in Figure 8, and the band structure of the bare Au(100) slab has been superimposed in dashed black lines. The band structure of the p(2×2) model is very similar to that of the bare Au(100) slab. The majority of the phosphorus contribution is located near the gold bands except for the big and lowly dispersive band around −0.2 eV, which is mostly a feature due to the interaction between the phosphorus atoms. The aforementioned flat band at 3.2 eV appears in blue, which confirms that it is mostly carried by the phosphorus atoms. Its shape is very similar to the flat band at 3.4 eV in the bare Au(100) slab, which indicates that it is a result of the hybridization of the phosphorus atoms with the gold atoms, as confirmed with the following PDOS and charge transfer analysis.

Using the calculated Löwdin charges in Quantum ESPRESSO, we find that after adsorption, each P atom has 5.475 valence electrons, which means that there is a transfer of +0.475 electrons from the Au surface to each P atom. The charge decomposition of the P atom (s = 1.8259, p = 3.6489, p_z = 1.2096, p_x = 1.2196, p_y = 1.2196) indicates that the charge transfer primarily occurs in the p orbitals, with a slight loss in the s orbital. This suggests an sp^3 hybridization of the P atoms and a strong covalent interaction with the underlying Au atoms, polarizing the Au−P bond. The four Au atoms surrounding the P atom lose 0.31 electrons each, primarily from their d orbitals with their s and p orbitals remaining almost unchanged. The charge decomposition of the d orbital of the topmost Au atoms is as follows: d_{z^2} = 1.9479, d_{xz} = 1.9195, d_{yz} = 1.9195, $d_{x^2-y^2}$ = 1.9061, and d_{xy} = 1.9238. The most depleted orbitals are the $d_{x^2-y^2}$, d_{xz} and d_{yz}.

The PDOS of the p(2×2) model was calculated for the phosphorus atoms and the gold atoms. Similarly to a previous study of the Hex-P monolayer on Au(111),[20] it appears that the peak at 3.2 eV (3.6 eV in the STS spectrum) is carried by the s and p_z orbitals of the phosphorus atoms (Figure 9b). The peak can be seen in both the PDOS of the s and p_z orbitals of the phosphorus atoms and is very similar to the thin peak of the STS spectrum.

The PDOS of the surface gold atoms (Figure 9a) shows peaks around 3.2 eV in the d_{xz} and d_{yz} orbitals and to a lesser extent in the d_{xy} orbitals. This confirms the strong interaction between the phosphorus atoms and surface gold atoms. We must notice that this result explains the p(2×2) surface structure but is not sufficient to explain the lifting of the Au-hex surface reconstruction. This interaction between the phosphorus atoms and the surface gold atoms generating a flat band around 3.2 eV and its corresponding peak in the LDOS is similar to what has been observed for the Hex-P monolayer on Au(111).[20]

Finally, an integrated LDOS calculation (ILDOS) has been performed around the peak at 3.2 eV, with an energy window from 2.90 to 3.40 eV. This ILDOS represents the spatial distribution of electronic states in this energy window. The results are shown in Figure 10. We can observe that the highest intensity of the ILDOS is located just below the phosphorus atoms, a location where the d_{xz} and d_{yz} orbitals of the surface gold atoms point toward. This indicates that the peak at 3.2 eV is carried notably by a mix of s and p_z orbitals of the phosphorus atoms and the d_{xz} and d_{yz} orbitals of the surface gold atoms (similar to the results for the Hex-P monolayer on Au(111)[20]), which is consistent with the PDOS analysis.

In summary, we have characterized the surface structure of phosphorus adsorbed on Au(100)-hex in the low-coverage regime. The observed p(2×2) superstructure arises from a strong modification of the initial reconstructed surface. We have demonstrated that the formation of this structure is

https://doi.org/10.1021/acs.jpclett.6c02046
J. Phys. Chem. Lett. 2026, 17, 9797−9806

accompanied by the lifting of the surface reconstruction and a quadrimerization of the gold atoms located beneath the phosphorus adatoms. The P−Au(100) interaction leads to a charge transfer from Au to P accompanied by a distinct peak above the Fermi level and involves the s and p_z orbitals of the phosphorus atoms. We hypothesize that the subsurface atomic strain, associated with this acceptor-like electronic state, will play a critical role in the nucleation and subsequent growth of phosphorus structures at higher coverages.

■ ASSOCIATED CONTENT

Supporting Information

The Supporting Information is available free of charge at https://pubs.acs.org/doi/10.1021/acs.jpclett.6c02046.

Additional experimental details and computational methods: sample preparation, low energy electron diffraction, STM and STS imaging and processing, grazing incidence X-ray diffraction, computational methods. Additional c(2×2) model. Supplementary large scale and high resolution STM images. (PDF)

■ AUTHOR INFORMATION

Corresponding Author

Yann Girard − *Laboratoire Matériaux et Phénomènes Quantiques CNRS-Université Paris Cité 10 rue Alice Domon et Léonie Duquet, Paris Cedex 13 75205, France;* orcid.org/0000-0001-5708-4338; Email: yann.girard@u-paris.fr

Authors

Mehdi Bouatou − *Laboratoire Matériaux et Phénomènes Quantiques CNRS-Université Paris Cité 10 rue Alice Domon et Léonie Duquet, Paris Cedex 13 75205, France; Max Planck Institute of Microstructure Physics, 06120 Halle, Germany*

Abhishek Karn − *Laboratoire Matériaux et Phénomènes Quantiques CNRS-Université Paris Cité 10 rue Alice Domon et Léonie Duquet, Paris Cedex 13 75205, France; Université Grenoble Alpes, CEA, Grenoble INP, IRIG, PHELIQS, 38000 Grenoble, France*

Cyril Chacon − *Laboratoire Matériaux et Phénomènes Quantiques CNRS-Université Paris Cité 10 rue Alice Domon et Léonie Duquet, Paris Cedex 13 75205, France*

Ian-Evan Michel − *CEA Paris-Saclay, DRF/IRAMIS//SPEC/GMT, 91191 Gif-sur-Yvette, France*

Yannick J. Dappe − *CEA Paris-Saclay, DRF/IRAMIS//SPEC/GMT, 91191 Gif-sur-Yvette, France; Université Paris-Saclay, CNRS, Centre de Nanosciences et de Nanotechnologies, 91120 Palaiseau, France;* orcid.org/0000-0002-1358-3474

Alexander Smogunov − *CEA Paris-Saclay, DRF/IRAMIS//SPEC/GMT, 91191 Gif-sur-Yvette, France*

Yves Garreau − *Laboratoire Matériaux et Phénomènes Quantiques CNRS-Université Paris Cité 10 rue Alice Domon et Léonie Duquet, Paris Cedex 13 75205, France; SOLEIL Synchrotron, L'Orme des Merisiers, 91190 Gif-sur-Yvette, France*

Alina Vlad − *SOLEIL Synchrotron, L'Orme des Merisiers, 91190 Gif-sur-Yvette, France;* orcid.org/0000-0001-7319-0093

Alessandro Coati − *SOLEIL Synchrotron, L'Orme des Merisiers, 91190 Gif-sur-Yvette, France*

Jérôme Lagoute − *Laboratoire Matériaux et Phénomènes Quantiques CNRS-Université Paris Cité 10 rue Alice Domon et Léonie Duquet, Paris Cedex 13 75205, France;* orcid.org/0000-0002-0568-6991

Complete contact information is available at: https://pubs.acs.org/10.1021/acs.jpclett.6c02046

Notes

The authors declare no competing financial interest.

■ ACKNOWLEDGMENTS

The authors thank the French National Research Agency (ANR-20-CE090023 DEFINE2D, ANR-22-CE09-0022 2DPhostrainE) for financial support.

■ REFERENCES

(1) Xia, F.; Wang, H.; Jia, Y. Rediscovering black phosphorus as an anisotropic layered material for optoelectronics and electronics. *Nat. Com.* **2014**, *5*, 1−6.

(2) Zhang, J. L.; Han, C.; Hu, Z.; Wang, L.; Liu, L.; Wee, A. T. S.; Chen, W. 2D Phosphorene: Epitaxial Growth and Interface Engineering for Electronic Devices. *Adv. Mater.* **2018**, *30*, 1802207.

(3) Guan, J.; Zhu, Z.; Tománek, D. Phase Coexistence and Metal-Insulator Transition in Few-Layer Phosphorene: A Computational Study. *Phys. Rev. Lett.* **2014**, *113*, 046804.

(4) Guo, H.; Lu, N.; Dai, J.; Wu, X.; Zeng, X. C. Phosphorene Nanoribbons, Phosphorus Nanotubes, and van der Waals Multilayers. *J. Phys. Chem. C* **2014**, *118*, 14051−14059.

(5) Ding, L.; Shao, P.; Yin, Y.; Ding, F. Synthesis of 2D Phosphorene: Current Status and Challenges. *Adv. Funct. Mater.* **2024**, *34*, 2316612.

(6) Bouatou, M.; Harsh, R.; Chacon, C.; Girard, Y.; Repain, V.; Bellec, A.; Rousset, S.; Smogunov, A.; Dappe, Y. J.; Lagoute, J. Black Phosphorus for Directed Molecular Assembly with Weak Electronic Coupling. *Adv. Mater. Interfaces* **2021**, *8*, 2101644.

(7) Harsh, R.; Mondal, S.; Sharma, D.; Bouatou, M.; Chacon, C.; Ilyn, M.; Rogero, C.; Repain, V.; Bellec, A.; Girard, Y.; et al. Identification and Manipulation of Defects in Black Phosphorus. *J. Phys. Chem. Lett.* **2022**, *13*, 6276−6282.

(8) Fourmental, C.; Mondal, S.; Banerjee, R.; Bellec, A.; Garreau, Y.; Coati, A.; Chacon, C.; Girard, Y.; Lagoute, J.; Rousset, S.; et al. Importance of Epitaxial Strain at a Spin-Crossover Molecule−Metal Interface. *J. Phys. Chem. Lett.* **2019**, *10*, 4103−4109.

(9) Fourmental, C.; Bellec, A.; Repain, V.; Lagoute, J.; Chacon, C.; Girard, Y.; Rousset, S.; Dappe, Y.; Vlad, A.; Resta, A.; et al. Deep metallic interdiffusion in a model ferromagnetic/molecular system. *Phys. Rev. Mater.* **2019**, *3*, 083603.

(10) Zhang, J. L.; Zhao, S.; Sun, S.; Wang, W.; Ma, Z.; Lian, X.; Li, Z.; Chen, W. Atom by Atom Condensation of Sn Single Clusters within Gold−Phosphorus Metal−Inorganic Porous Networks. *J. Phys. Chem. Lett.* **2021**, *12*, 745−751.

(11) Celis, A.; Nair, M. N.; Sicot, M.; Nicolas, F.; Kubsky, S.; Malterre, D.; Taleb-Ibrahimi, A.; Tejeda, A. Superlattice-induced minigaps in graphene band structure due to underlying one-dimensional nanostructuration. *Phys. Rev. B* **2018**, *97*, 195410.

(12) Sun, S.; You, J.-Y.; Cai, Z.; Su, J.; Yang, T.; Peng, X.; Wang, Y.; Geng, D.; Gou, J.; Huang, Y.; et al. 1D Flat Bands in Phosphorene Nanoribbons with Pentagonal Nature. *Adv. Mater.* **2025**, *37*, 2411182.

(13) Sun, S.; Yang, T.; Ma, Z.; Ding, H.; Zhao, S.; Hu, J.; Xu, Q.; Lian, X.; Gu, C.; Li, Z.; et al. Experimental Realization of One-Dimensional Metal-Inorganic Chain: Gold−Phosphorus Chain. *ACS Materials Lett.* **2020**, *2*, 873−879.

(14) Zhang, J. L.; Zhao, S.; Sun, S.; Niu, T.; Zhou, X.; Gu, C. D.; Han, C.; Yuan, K. D.; Guo, R.; Wang, L.; et al. Phosphorus Nanostripe Arrays on Cu(110): A Case Study to Understand the Substrate Effect on the Phosphorus thin Film Growth. *Adv. Mater. Interfaces* **2017**, *4*, 1601167.

(15) David, J.; Jeřábek, F.; Procházka, P.; Černý, M.; Ciobanu, C. V.; Průša, S.; Šikola, T.; Kodambaka, S.; Kolíbal, M. Direct Observation of Structural Phase Transformations during Phosphorene Formation on Cu(111). *ACS Nano* **2025**, *19*, 4289−4298.
(16) Del Puppo, S.; Biasin, P.; Sala, A.; Mantegazza, P.; Pasqua, I.; Ghidorsi, E.; Caporali, M.; Resta, A.; Coati, A.; Genuzio, F.; et al. Blue phosphorene on Au(111): theoretical, spectroscopic and diffraction analysis reveal the role of single Au adatoms. *Nanoscale Adv.* **2024**, *6*, 3582−3589.
(17) Zhang, W.; Enriquez, H.; Tong, Y.; Mayne, A. J.; Bendounan, A.; Dappe, Y. J.; Kara, A.; Dujardin, G.; Oughaddou, H. Phosphorus Pentamers: Floating Nanoflowers form a 2D Network. *Adv. Funct. Mater.* **2020**, *30*, 2004531.
(18) Chahib, O.; Yin, Y.; Liu, J.-C.; Li, C.; Glatzel, T.; Ding, F.; Yuan, Q.; Meyer, E.; Pawlak, R. Probing charge redistribution at the interface of self-assembled cyclo-P5 pentamers on Ag(111). *Nat. Commun.* **2024**, *15*, 6542.
(19) Xu, J.-P.; Zhang, J.-Q.; Tian, H.; Xu, H.; Ho, W.; Xie, M. One-dimensional phosphorus chain and two-dimensional blue phosphorene grown on Au(111) by molecular-beam epitaxy. *Phys. Rev. Mater.* **2017**, *1*, 061002.
(20) Karn, A.; Michel, I.-E.; Lezoualc'h, M.; Chacon, C.; Girard, Y.; Smogunov, A.; Dappe, Y. J.; Lagoute, J. Probing Surface-Mediated Electronic Coupling in Flat Hexagonal Phosphorus Nanostructures and Monolayer on Au(111). *Small* **2024**, *20*, 2405924.
(21) Zhou, D.; Meng, Q.; Si, N.; Zhou, X.; Zhai, S.; Tang, Q.; Ji, Q.; Zhou, M.; Niu, T.; Fuchs, H. Epitaxial Growth of Flat, Metallic Monolayer Phosphorene on Metal Oxide. *ACS Nano* **2020**, *14*, 2385−2394.
(22) Schaal, M.; Picker, J.; Otto, F.; Gruenewald, M.; Forker, R.; Fritz, T. An alternative route towards the fabrication of 2D blue phosphorene. *J. Phys.: Condens. Matter* **2021**, *33*, 485002.
(23) Hammer, R.; Sander, A.; Förster, S.; Kiel, M.; Meinel, K.; Widdra, W. Surface reconstruction of Au(001): High-resolution real-space and reciprocal-space inspection. *Phys. Rev. B* **2014**, *90*, 035446.
(24) Ercolessi, F.; Tosatti, E.; Parrinello, M. Au (100) Surface Reconstruction. *Phys. Rev. Lett.* **1986**, *57*, 719−722.
(25) Havu, P.; Blum, V.; Havu, V.; Rinke, P.; Scheffler, M. Large-scale surface reconstruction energetics of Pt(100) and Au(100) by all-electron density functional theory. *Phys. Rev. B* **2010**, *82*, 161418.
(26) Zhang, E.; Lu, H.; Zhang, W.; Cao, S.; Wang, Y.; Rong, R.; Liu, Y.; Zhang, Z.; Yang, M.; Liu, Y.; et al. Lifting surface reconstruction of Au (100) by tellurium adsorption. *Nano Res.* **2023**, *16*, 6967−6973.
(27) Tempas, C. D.; Skomski, D.; Tait, S. L. Lifting of the Au(100) surface reconstruction by Pt, Cr, Fe, and Cu adsorption. *Surf. Sci.* **2016**, *654*, 33−38.
(28) Jiang, Y.; Liang, X.; Ren, S.; Chen, C.-L.; Fan, L.-J.; Yang, Y.-W.; Tang, J.-M.; Luh, D.-A. The growth of sulfur adlayers on Au(100). *J. Chem. Phys.* **2015**, *142*, 064708.
(29) Andryushechkin, B.; Pavlova, T.; Eltsov, K. Adsorption of halogens on metal surfaces. *Surf. Sci. Rep.* **2018**, *73*, 83−115.
(30) Barzaga, R.; Martínez, J. A.; Farías, M. H.; Hernández, M. P. From the Terrace Contraction to the Hexameric Sulfur Phase in the Au(100) Surface: A Combined Density Functional Theory and Scanning Tunneling Microscopy Study. *J. Phys. Chem. C* **2019**, *123*, 12183−12194.
(31) Tsvetanova, M.; Syromyatnikov, A. G.; Van Der Meer, T.; Van Houselt, A.; Zandvliet, H. J. W.; Klavsyuk, A. L.; Sotthewes, K. Self-Assembled Decanethiolate Monolayers on Au(001): Expanding the Family of Known Phases. *Langmuir* **2022**, *38*, 10202−10215.
(32) Zhang, W.; Enriquez, H.; Zhang, X.; Mayne, A. J.; Bendounan, A.; Dappe, Y. J.; Kara, A.; Dujardin, G.; Oughaddou, H. Blue Phosphorene Reactivity on the Au(111) Surface. *Nanotechnology* **2020**, *31*, 495602.
(33) Zhang, X.; El Kari, H.; Enriquez, H.; Bendounan, A.; Kara, A.; Dappe, Y. J.; Oughaddou, H. Synthesis and Properties of Phosphorus Nanostructures on Au(110). *Nanoscale* **2024**, *16*, 21088−21095.
(34) Giannozzi, P.; Baroni, S.; Bonini, N.; Calandra, M.; Car, R.; Cavazzoni, C.; Ceresoli, D.; Chiarotti, G. L.; Cococcioni, M.; Dabo, I.; et al. QUANTUM ESPRESSO: A Modular and Open-Source Software Project for Quantum Simulations of Materials. *J. Phys.: Condens. Matter* **2009**, *21*, 395502.
(35) Giannozzi, P.; Andreussi, O.; Brumme, T.; Bunau, O.; Nardelli, M. B.; Calandra, M.; Car, R.; Cavazzoni, C.; Ceresoli, D.; Cococcioni, M.; et al. Advanced capabilities for materials modelling with QUANTUM ESPRESSO. *J. Phys.: Condens. Matter* **2017**, *29*, 465901.
(36) Electron Work Function of the Elements. https://public.wsu.edu/~pchemlab/documents/Work-functionvalues.pdf.
(37) Dougherty, D. B.; Maksymovych, P.; Lee, J.; Feng, M.; Petek, H.; Yates, J. T. Tunneling spectroscopy of Stark-shifted image potential states on Cu and Au surfaces. *Phys. Rev. B* **2007**, *76*, 125428.
(38) Popescu, V.; Zunger, A. Extracting E versus k effective band structure from supercell calculations on alloys and impurities. *Phys. Rev. B* **2012**, *85*, DOI: 10.1103/PhysRevB.85.085201
(39) Pacilè, D.; Cardoso, C.; Avvisati, G.; Vobornik, I.; Mariani, C.; Leon, D. A.; Bonfà, P.; Varsano, D.; Ferretti, A.; Betti, M. G. Narrowing of d bands of FeCo layers intercalated under graphene. *Appl. Phys. Lett.* **2021**, *118*, 121602.

https://doi.org/10.1021/acs.jpclett.6c02046
J. Phys. Chem. Lett. 2026, 17, 9797−9806